

## CIRUMGALACTIC OXYGEN ABSORPTION AND FEEDBACK

WILLIAM G. MATHEWS<sup>1</sup> AND J. XAVIER PROCHASKA<sup>1</sup>

*Draft version July 26, 2021*

### ABSTRACT

OVI absorption in quasar spectra caused by intervening circumgalactic atmospheres suggests a downturn in the atmospheric column density in sightlines passing beyond about 100 kpc from central star-forming galaxies. This turnover supports the hypothesis that the oxygen originates in the central galaxies. When converted into oxygen space density using an Abel integral inversion, the OVI columns require  $\gtrsim 10^9 M_\odot$  of oxygen concentrated near 100 kpc. Circumgalactic gas within this radius cools in less than 1 Gyr and radiates  $\sim 10^{42.2}$  erg s<sup>-1</sup> overall. The feedback power necessary to maintain such oxygen-rich atmospheres for many Gyrs cannot be easily supplied by galactic supernovae. However, massive central black holes in star-forming galaxies may generate sufficient accretion power and intermittent shock waves at  $r \sim 100$  kpc to balance circumgalactic radiation losses in late-type  $L^*$  galaxies. The relative absence of OVI absorption observed in early-type, passive  $L^*$  galaxies may arise from enhanced AGN feedback from their more massive central black holes.

*Subject headings:* galaxies: abundances — quasars: absorption lines

### 1. INTRODUCTION

The possibility of high oxygen abundances in hot, virialized gas around normal star-forming galaxies has attracted much attention. Tumlinson et al. (2011) describe strong UV absorption in quasar spectra due to the OVI doublet (1031.9, 1037.6Å) having redshifts similar to those of  $\sim L^*$  galaxies observed close to quasar sightlines. Distances between sightlines and the central galaxies, i.e. the impact parameters  $R$ , are large, implying that the absorption occurs in extended circumgalactic gaseous atmospheres surrounding star-forming galaxies. Impact parameters of  $10 \lesssim R \lesssim 150$  kpc are observed in star-forming galaxies with redshifts  $0.1 \lesssim z_{gal} \lesssim 0.4$  and stellar masses  $9.5 \lesssim \log(M_*/M_\odot) \lesssim 11.5$ . Large oxygen column densities  $N_{\text{OVI}} \approx 10^{14.5 \pm 0.25}$  cm<sup>-2</sup> suggest large oxygen masses.

Detailed observations of circumgalactic absorption by O<sup>+5</sup> and other ions of C, N, O, Mg, Si, and Fe are described in a series of publications: Werk et al. (2012,2013,2014,2016), Johnson, Chen, and Mulchaey (2015  $\equiv$  JCM), Borthakur et al. (2016). Broad OVI absorption is detected in essentially all sightlines near star-forming galaxies, but in only a small fraction of sightlines near passive, early-type  $L^*$  galaxies. Of interest here are decreasing O VI absorption columns that extend beyond the  $\sim 150$  kpc survey limit of Tumlinson et al. to at least  $\sim 300$  kpc around  $L^*$  galaxies (Prochaska et al. 2011; JCM).

Meanwhile, a significant computational effort is underway by cosmological simulators to understand the origin of oxygen in the hot circumgalactic gas: Stinson et al. (2013); Suresh, et al. (2015); Liang, Kravtsov & Agertz (2016); Roca-Fabrega et al. (2016); Oppenheimer, et al. (2016); Sokolowska et al. (2016) etc. In these studies most of the circumgalactic oxygen is provided by supernova-driven galactic winds from the central galaxy.

Nevertheless, many of these sophisticated computational studies underpredict observed OVI column densities.

Recent theoretical treatments of O VI in the circumgalactic medium include the phenomenological model of Stern et al. (2016) which envisions O VI as low-density, externally photoionized gas surrounding denser ionized gaseous clumps that produce lower ionization absorption lines of C, N, O, Mg, Si, and Fe. This scenario explicitly links the kinematics of the O VI gas with the lower ionization material (as suggested by observations of Werk et al. 2016). Most recently, Faerman et al. (2016) introduce a model for galaxy coronae to reproduce O VI observations together with X-ray observations of higher ionization states of oxygen in the Milky Way. In their phenomenological model, circumgalactic gas is multi-phase with a distribution of densities all in pressure equilibrium.

As with lower ionization absorption lines, some OVI absorption may occur in small, actively cooling regions. However, as seen in Figure 3 of Werk et al. (2013), broad velocity widths of OVI absorption lines extend to velocities unassociated with low ionization absorption. This suggests that most OVI absorption arises not in thermally perturbed regions but in extended hydrostatic atmospheres – we adopt this assumption here.

In what follows we pursue the astrophysical implications of the observed OVI column density profile  $N_{\text{OVI}}(R)$ , assuming that the oxygen has been expelled from the central star-forming galaxies and now resides in circumgalactic atmospheres in collisional ionization equilibrium. Specifically, we create simple hot gas atmospheres around a fiducial  $L^*$  galaxy with a stellar mass  $M_* = 10^{10.4} M_\odot$  near the center of the sample observed by Tumlinson et al. (2011), having a dark halo mass  $M_h = 10^{12.2} M_\odot$ . We begin with a reference atmosphere devoid of feedback distortion in which the gas has an NFW profile reduced by the cosmic baryon fraction. From this we construct several approximate atmospheres distorted by increasing amounts of feedback heating which must be maintained by continued feed-

<sup>1</sup> University of California Observatories/Lick Observatory, Department of Astronomy and Astrophysics, University of California, Santa Cruz, CA 95064 (mathews@ucolick.org).

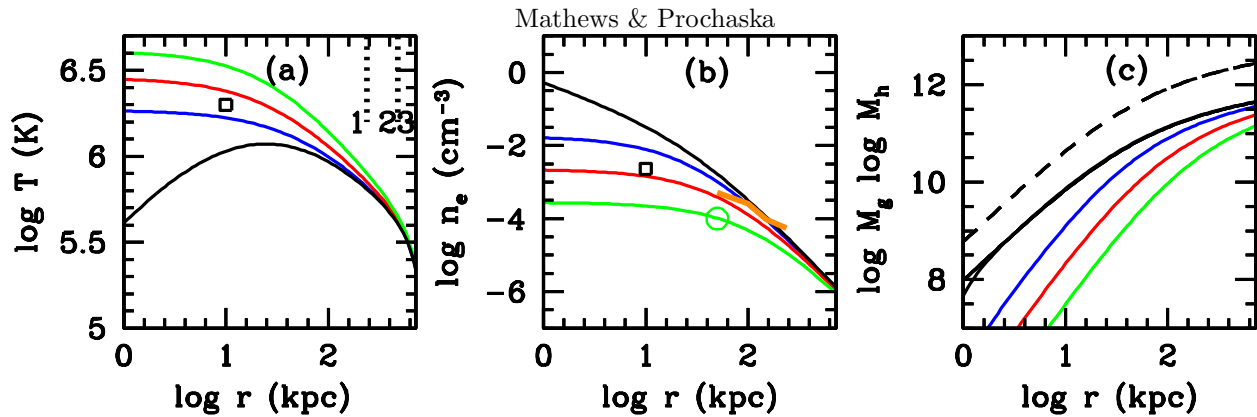


FIG. 1.— Four atmospheres in the  $L^*$  potential. *Black*: no-feedback atmosphere with reduced NFW profile, *Blue, Red and Green*: three atmospheres with increasing feedback heating and distortion. (a) Temperature profiles. Radii at 1, 2 and 3  $r_{200}$  marked at upper right. (b) gas density profiles. *Orange line*:  $L^*$   $n_e(r)$  profile for  $50 < r < 240$  kpc from Oppenheimer et al. (2016). (c) dark halo (*dashed line*) and cumulative gas mass profiles in  $M_\odot$ . Black squares are Milky Way density and temperature at  $r_{kpc} = 10$  from Miller & Bregman (2016).

back that balances radiation losses. The radial oxygen abundance profile in each atmosphere is adjusted until the space density profile of  $O^{+5}$  ions is consistent with the observed mean column density profile  $N_{OVI}(R)$ . We show that the local O abundance can significantly exceed solar at  $\sim 100$  kpc with large total oxygen masses  $\gtrsim 10^9 M_\odot$ . Radiative cooling time profiles are almost identical for all model atmospheres, but their radiative luminosities require feedback energies in excess of that expected from supernova feedback alone. This provides strong evidence that central black holes are the dominant source of feedback energy having black hole accretion rates and masses that match those expected in  $L^*$  galaxies.

## 2. HYDROSTATIC CIRCUMGALACTIC ATMOSPHERES

Following Oppenheimer et al. (2016), we adopt a representative  $L^*$  central galaxy having stellar mass  $M_\star = 10^{10.4} M_\odot$  and dark halo mass  $M_h = 10^{12.2} M_\odot$ . The NFW halo that confines the hot gas is assumed to have concentration  $c = 4.86(M_{200}/10^{14} M_\odot)^{-0.11} = 7.67$  (Neto et al. 2007), and virial radius  $r_{200} = 240$  kpc where the density is 1/200 of the critical density. We expect that dark halos in  $L^*$  galaxies are no longer accreting dark (or baryonic) matter and may have been quiescent for several Gyrs (Prada et al. 2006; Cuesta et al. 2008; Diemer & Kravtsov 2014). Consequently, we adopt an NFW density profile for the dark matter halo, and assume that it has not changed substantially since redshifts  $z \sim 0.2$  where most circumgalactic OVI absorption is observed.

We now construct several approximate atmospheres in this halo having increasing amounts of distortion due to feedback. The equation of hydrostatic equilibrium  $dP/dr = -\rho g_{NFW}$  can be written

$$dT/dr = -(T/r)(d \log \rho / d \log r) - g_{NFW}(\mu m_p / k) \quad (1)$$

where  $P = (k/\mu m_p)\rho T$ ,  $m_p$  is the proton mass and  $\mu = 0.61$  is the molecular weight. In the absence of feedback, baryons also have an NFW density profile reduced by the cosmic baryon fraction,  $f_b = 0.16$ . We disregard the stellar mass of the central galaxy since it is only  $\sim 10$  percent of the baryonic mass within the virial radius. The gas density profile without feedback is therefore  $\rho(r) = f_b \rho_0 / y(1+y)^2$  where  $y = c(r/r_{200})$ ,  $\rho_0 = (200\rho_c/3)c^3/f(c)$ ,  $f(y) = \ln(1+y) - y/(1+y)$ , and  $\rho_c = 9.2 \times 10^{-30}$  gm cm $^{-3}$  is the critical density

for Hubble constant  $H_0 = 70$  km s $^{-1}$ . The halo mass is  $M_h = M_{200} = (4\pi/3)200\rho_c r_{200}^3$  and the gravitational acceleration  $g_{NFW} = GM_h(r)/r^2$ .

In the presence of feedback, atmospheric gas is heated, its central entropy is increased and the entire atmosphere is pushed outward. To mimic these feedback effects, we consider density profiles described by

$$\rho = f_b \rho_0 / (y_0 + y)^3 \quad (2)$$

where  $y_0$  is a parameter that increases with the influence of feedback. The central entropy  $S = T/n_e^{2/3}$  has zero slope similar to galaxy group profiles visible in X-rays (Pratt et al. 2010). Since feedback sources are centrally concentrated, these atmospheres are designed to approach the feedback-free density profile at large radius,  $\rho(y) \approx f_b \rho_0 / y^3$ . We therefore disregard any significant density change at large radius, either an enhancement as gas is pushed out by feedback or a gas deficiency if feedback extends to the distant halo. In any case, intermediate radii,  $\sim 100$  kpc, are most relevant to our concerns here. Our adoption of equation (2) does not affect conclusions discussed below.

Solid black contours in Figure 1 show temperature, density, and gas mass profiles for a circumgalactic atmosphere without feedback. Also in Figure 1 are profiles for three atmospheres with increasing feedback:

$$\text{blue} : \text{red} : \text{green} :: y_0 = 1 : 2 : 4 \quad (3)$$

Atmospheric structural distortion is stabilized when the time-averaged feedback power maintains atmospheric profiles against radiation losses. If feedback drops below this maintenance level, large masses of gas can cool toward the central galaxy, resulting in an unphysical mass accumulation, similar to the overcooling problem encountered in cosmological simulations. Structural and maintenance feedback can be provided by the same physical mechanisms.

The green atmosphere in Figure 1 is designed to match a hot gas density of  $10^{-4}$  cm $^{-3}$  at radius  $\sim 50$ -60 kpc in the Milky Way as suggested by Fang et al. (2013) from XMM surface brightness observations and by Sokolowska et al. (2016) from OVII and OVIII observations. This density is marked with a green circle in Figure 1b.

3. O<sup>+5</sup> COLUMN AND SPACE DENSITIES

Blue squares in Figure 2a are COS-Halos detections of OVI column densities  $N_{\text{OVI}}$  in circumgalactic atmospheres of  $L^*$  galaxies (Tumlinson et al. 2011) at sightline offsets  $R$  in kpc. While most columns are clustered about  $N_{\text{OVI}} \sim 10^{14.7} \text{ cm}^{-2}$ , there is evidence of decreasing columns beyond  $R \sim 100$  kpc. This decrease is confirmed by additional OVI observations by JCM, many having larger  $R$ . In Fig. 2a we plot JCM data for star-forming  $L^*$  galaxies having impact offsets  $R > 75$  kpc, and stellar masses within  $10.1 < \log(M_*/M_\odot) < 10.7$ . While only two galaxies are detected (green squares in Figure 2), a large number of upper limits (inverted red triangles) provides convincing evidence of a rather sharp decrease in OVI columns beyond  $\sim 100$  kpc. Such a decrease strongly supports the prevailing interpretation that very large oxygen masses have been ejected from  $L^*$  galaxies and/or their progenitors. Decreasing  $N_{\text{OVI}}(R)$  profiles also constrain the atmospheric O/H abundance and the feedback mechanism that maintains it.

Although data are sparse, we fashion a magenta line in Figure 2 showing a likely column density profile for  $L^*$  galaxies. The magenta line is described by

$$N_{\text{OVI}} = N_0 [1 + (R/R_0)^p]^{-1} (R/R_1)^q \quad (4)$$

where  $N_0 = 5.2 \times 10^{14} \text{ cm}^{-2}$ ,  $R_1 = 40$  kpc,  $q = -1/3$ ,  $R_0 = 140$  kpc and  $p = 3$ .

The corresponding empirical space density of O<sup>+5</sup> ions  $\tilde{n}_{\text{O}^{+5}}(r)$ , can be found from an Abel integral inversion,

$$\tilde{n}_{\text{O}^{+5}}(r) = -\frac{1}{\pi} \int_r^\infty \frac{dN}{dR} \frac{dR}{(R^2 - r^2)^{1/2}}$$

which is plotted as a magenta line in Figure 2b. The inner, dotted part of the  $\tilde{n}_5 \equiv \tilde{n}_{\text{O}^{+5}}(r)$  profile is unconstrained by current  $N_{\text{OVI}}$  data. For comparison, dashed lines in Figure 2b shows O<sup>+5</sup> space density profiles  $n_5(r)$  for each atmosphere in Fig. 1, assuming uniform solar abundance  $A_{\text{O}\odot} = 5 \times 10^{-4}$  and employing ionic fractions for collisional ionization equilibrium (Gnat and Sternberg 2007).

The juxtaposition of  $n_5$  and  $\tilde{n}_5$  profiles in Figure 2b allows an instant determination of atmospheric O abundance profiles  $Z_{\text{O}}(r)$  in solar units required to match the mean profile  $\tilde{n}_5(r)$  and, when projected, the adopted mean column density profile  $N_{\text{OVI}}(R)$  in Figure 2a. For example, the oxygen abundance in solar units for the red atmosphere is simply  $Z_{\text{O},\text{red}}(r) = \tilde{n}_5(r)/n_{5,\text{red}}(r)$  at every radius.

Oxygen abundance profiles derived in this manner for each atmosphere are illustrated in Figure 3a. Maximum abundances are expected near  $r \sim 100$  kpc where the slope  $dN_{\text{OVI}}/dR$  changes. Oxygen abundances  $Z_{\text{O}}$  are large, particularly in the high feedback, low density green atmosphere. At  $r = 100$  kpc, O abundances in the blue, red and green atmospheres are  $Z_{\text{O}} = 1.1, 2.6$  and  $8.5$  solar respectively. The cumulative oxygen mass shown in Figure 3b also increases with feedback in the blue, red and green atmospheres, totaling 0.84, 1.08 and 1.61 (in units of  $10^9 M_\odot$ ) respectively. In a closed box model an  $M_* = 10^{10.4} M_\odot$  stellar mass can produce an oxygen mass of only  $\sim 10^8 M_\odot$  (Zahid et al. 2012). However, in the simulation of Oppenheimer et al. (2016) the total

oxygen mass within  $r_{200}$  at zero redshift is  $3 \times 10^8 M_\odot$ , but their computed sightline column densities  $N_{\text{OVI}}$  are about 3 times lower than those observed and the space density of O ions is not as concentrated near  $r \sim 100$  kpc as we require here.

In Figure 4a we show the remarkable similarity of cooling time profiles  $t_{\text{cool}}(r)$  for all atmospheres. It is easy to show that this similarity follows from the relation  $Z_{\text{O}} = \tilde{n}_5/n_5$  when oxygen dominates the metallicity,  $Z \approx Z_{\text{O}}$ . Therefore, the cooling time profile holds for any  $L^*$  atmosphere, not just those proposed here.

Large bolometric X-ray luminosity profiles in Figure 4b,  $\log L_X \approx 42.2 \pm 0.4 \text{ erg s}^{-1}$ , attest to the powerful cooling effect of  $\sim 10^9 M_\odot$  of oxygen extending to  $r \approx 100$  kpc. To explore the destiny of pure cooling without feedback, we computed spherical time-dependent cooling flows allowing blue, red and green (b,r,g) atmospheres initially at rest to evolve for the lookback time 2.4 Gyrs at redshift 0.2 with abundances from Fig. 3a. These straightforward calculations, not discussed in detail here, verify that gas masses of  $\log(M/M_\odot) \approx (11.2, 10.9$  and  $10.5)$ , all in excess of  $M_*$ , cool at the origin in (b,r,g) atmospheres during this relatively short time. All oxygen-rich gas within  $\approx 210$  kpc cools. Such an atmospheric collapse is not supported by the recent star formation history of the Milky Way (Gonzalez et al. 2017) or by observations of extended circumgalactic OVI absorption in star-forming  $L^*$  galaxies. Clearly, a strong time-averaged maintenance feedback power comparable to  $L_X$  must be provided by supernovae or central black holes. Our concern here is not the energetics of the outflows that previously carried O-rich gas out to  $\sim 100$  kpc, but how this gas is maintained during more recent times.

In the figures we assume that oxygen is completely mixed on atomic scales, but the degree of mixing remains uncertain. It is likely that circumgalactic oxygen is inhomogeneous, which would decrease the radiative cooling time below that in Figure 4a, causing small, O-rich regions to cool locally, perhaps even in the presence of maintenance feedback. Such local cooling is supported by low-ionization circumgalactic absorption lines in quasar spectra.

Core-collapse supernovae in late type  $L^*$  galaxies occur at a rate of 1-3 per century, but generate only  $\sim 0.6 \times 10^{42} \text{ erg s}^{-1}$ , most of which is dissipated locally in strong shocks in the galactic disk. Successful  $L^*$  feedback requires intermittent shocks propagating through gas at  $r \sim 100$  kpc at some mean interval  $\Delta t$ . The rate that entropy is radiated away by gas at  $r = 100$  kpc (where  $n \approx 10^{-4} \text{ cm}^{-3}$ ,  $T \approx 10^6 \text{ K}$  and  $Z \approx Z_\odot$ ) can be restored by shocks every  $\log \Delta t = (7, 8, 9)$  yrs with large Mach numbers (1.25, 1.7, 3.9), roughly similar to feedback shock strengths in galaxy group atmospheres. Even if supernova power were sufficient, neither stochastic variations in the galactic supernova rate nor slowly moving (forward and reverse) shocks expected in sustained supernova-driven winds are sufficiently intermittent.

Consequently, massive central black holes may be the most promising source of distant, intermittent feedback shocks. Following King and Pounds (2015), fast-wind feedback from AGNs having luminous accretion disks generate mechanical luminosities  $\sim 0.05 L_E$  where  $L_E = 1.26 \times 10^{38} (M_\bullet/M_\odot) \text{ erg s}^{-1}$  is the Eddington luminosity.

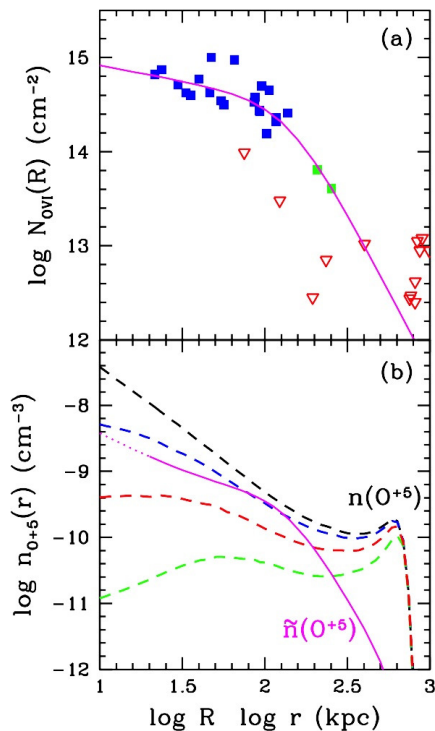


FIG. 2.— (a)  $N_{\text{OVI}}$  observations. Blue squares from COS-Halos, green squares and red upper limits from JCM. (b) Dashed lines:  $n_{\text{O}^{+5}}(r)$  profiles for the four atmospheres, all with solar abundance. Magenta line:  $\bar{n}_{\text{O}^{+5}}(r)$  profile.

Since central black holes in  $L^*$  galaxies with  $M_* = 10^{10.4} M_\odot$  have masses  $M_\bullet$  similar to that in the Milky Way,  $4.5 \times 10^6 M_\odot$ , the expected mechanical power of  $L^*$  winds is  $\sim 30 \times 10^{42} \sim 30 L_X$  erg s $^{-1}$ . This is sufficient to balance X-ray luminosities in Figure 4b with central AGNs that are intermittently active only 3 percent of the time. This duty cycle is  $\lesssim 10$  percent as required by Oppenheimer et al. (2017) to enhance OVI-absorbing ions in atmospheres of  $L^*$  galaxies.

More collimated feedback modes may also be present. In galaxy groups, having black holes and dark halo masses roughly ten times larger than in  $L^*$  galaxies, the accretion power of central black holes maintain atmospheric temperatures  $T \sim 10^7$  K with no evidence of recent star formation or luminous accretion disks. In addition, the Fermi bubbles in the Milky Way reveal that its central black hole is currently delivering an (albeit uncertain) energy of  $\sim 10^{59}$  ergs to the circum-Galactic atmosphere (Guo & Mathews 2012, Guo et al. 2012), equivalent to the total Galactic supernova energy generated in  $10^8$  yrs. Since outward propagaing shocks in atmospheres with  $d \log \rho / d \log r > -2$  naturally weaken,

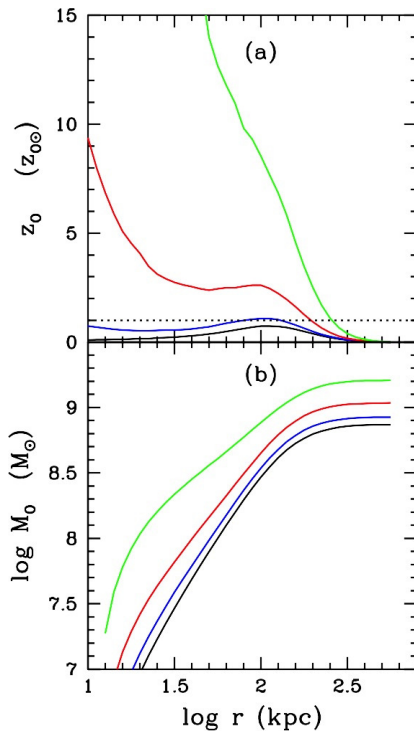


FIG. 3.— (a) Oxygen abundance profiles in solar units required for each atmosphere; Dotted line marks solar abundance. (b) Cumulative oxygen mass profiles.

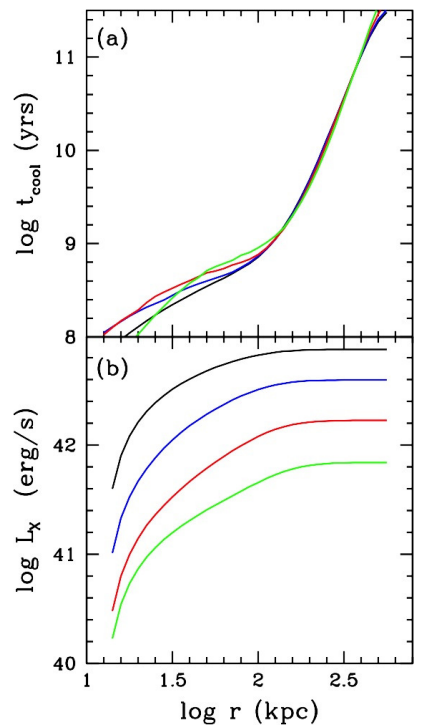


FIG. 4.— (a) Short cooling time profiles for each atmosphere. (b) Cumulative bolometric luminosity profiles of each atmosphere, emitted primarily at energies  $< 0.5$  keV.

shocks formed at large radii by collimated black hole outflows provide more efficient feedback. The non-thermal content of the Fermi Bubbles and extragalactic jets may also suggest feedback modes stronger than disk winds.

Further evidence that central black holes may energize circumgalactic gas are much lower OVI absorption columns observed in non-starforming passive  $L^*$  galaxies (Tumlinson et al. 2011). Since central black holes in passive  $L^*$  galaxies are on average  $\sim 40$  times more massive than those in star-forming  $L^*$  galaxies (Reines & Volonteri 2015), the accretion feedback in passive galaxies may drive most of the OVI-absorbing circumgalactic gas entirely out of the galactic potential. Upper limits of four star-forming  $L^*$  galaxies in Figure 2a also lie far below the magenta profile. Perhaps unusually large feedback events with energy  $\gtrsim (GM_g M_h / r)|_{100 \text{ kpc}} \sim 10^{58.7}$  ergs have removed the entire atmosphere.

We acknowledge a very helpful observational communication from Todd Tripp and useful remarks from Fabrizio Brighenti. WGM thanks George Poultsides, John Harris, Joseph Palascak and Francisco Rhein for sustaining support.

## REFERENCES

- Borthakur, S., Heckman, T., Tumlinson, J., et al. 2015, ApJ, 813, 46  
 Cuesta, A. J., Prada, F., Klypin, A., Moles, M. 2008 MNRAS 389 385  
 Diemer, B., Kravtsov, A. V., 2014 ApJ 789, 1  
 Faerman, Y., Sternberg, A., McKee, C. F. 2016, (arXiv160200689F)  
 Fang, T.; Bullock, J.; Boylan-Kolchin, M. 2013, ApJ 762, 20  
 Gnat, O. & Ferland, G. J. 2012, ApJ 199, 20  
 Gnat, O. & Sternberg, A. 2007 ApJS 168, 213  
 Gonzalez Delgado, R. M. et al. 2017, arXiv170606119  
 Guo, F., Mathews, W. G., Dobler, G., Oh, S. P. 2012, ApJ 756, 182  
 Guo, F., Mathews, W. G. 2012, ApJ, 756, 181  
 Johnson, S. D., Chen, H.-W., & Mulchaey, J. S. 2015, MNRAS, 449, 3263  
 King, A. R; Pounds, K. A. 2015, ARA&A, 53, 115.

- Liang, C. J., Kravtsov, A. V., Agertz, O. 2016 MNRAS 488, 1164
- Miller, M. J.; Bregman, J. N. 2016, ApJ 829, 9.
- Neto, A. F. et al. 2007, MNRAS 381, 1450
- Oppenheimer, B. D. et al. 2016 MNRAS 460, 2157
- Oppenheimer, B. D. et al. 2017 (arXiv170507897).
- Prada, F., et al. 2006, ApJ 645 1001
- Pratt, G. W. et al. 2010, A&A 511, A85
- Prochaska, J. X., Weiner, B., Chen, H.-W., Mulchaey, J., & Cooksey, K. 2011, ApJ, 740, 91
- Reines, A. E., Volonteri, M. ApJ 2015 813, 82
- Roca-Fabrega, S. et al. 2016, ApJ, 824, 94
- Sokolowska, A., Mayer, L<sub>j</sub> Balbul, A., Madau, P., Shen, S. 2016, ApJ, 819, 21
- Stern, J., Hennawi, J. F., Prochaska, J. X., & Werk, J. K. 2016, ArXiv e-prints, arXiv:1604.02168
- Stinson, G. C., Brook, C, Prochaska, J. X. et al. 2013, MNRAS 425, 1270
- Suresh, J., Rubin, K. H. R., Kannan, R., Werk, J. K., Hernquist, L, Vogelsberger, M. 2015 (arXiv151100687S)
- Tumlinson, J., et al. 2011, Science 334, 948
- Werk, J. K., Prochaska, J. X., et al. 2016,(arXiv160900012W)
- Werk, J. K., Prochaska, J. X., et al. (2014), ApJ 792, 8
- Werk, J. K., Prochaska, J. X., Thom, C., Tumlinson, J., Tripp, T. M., O'Meara, J. M., Peebles, M. S., 2013, ApJS, 2014, 17
- Werk, J. K., Prochaska, J. X., Thom, C., Tumlinson, J., Tripp, T.M., O'Meara, J. M., Meiring, J. D. (2012), ApJS 198, 3
- Zahid, H. J., Dima, G. I., Kewley, L. J., Erb, D. K., Dave, R. 2012, ApJ 757, 54